Volume of Bone Metastasis Assessed with Whole-Body Diffusion-weighted Imaging Is Associated with Overall Survival in Metastatic Castration-resistant Prostate Cancer[1]

Raquel Perez-Lopez, MD, MSc
David Lorente, MD
Matthew D. Blackledge, PhD
David J. Collins, BA, CPhys
Joaquin Mateo, MD, MSc
Diletta Bianchini, MD
Aurelius Omlin, MD
Andrea Zivi, MD
Martin O. Leach, PhD
Johann S. de Bono, MD, PhD
Dow-Mu Koh, MD
Nina Tunariu, MD, FRCR, MRCP

Purpose: To determine the correlation between the volume of bone metastasis as assessed with diffusion-weighted (DW) imaging and established prognostic factors in metastatic castration-resistant prostate cancer (mCRPC) and the association with overall survival (OS).

Materials and Methods: This retrospective study was approved by the institutional review board; informed consent was obtained from all patients. The authors analyzed whole-body DW images obtained between June 2010 and February 2013 in 53 patients with mCRPC at the time of starting a new line of anticancer therapy. Bone metastases were identified and delineated on whole-body DW images in 43 eligible patients. Total tumor diffusion volume (tDV) was correlated with the bone scan index (BSI) and other prognostic factors by using the Pearson correlation coefficient (r). Survival analysis was performed with Kaplan-Meier analysis and Cox regression.

Results: The median tDV was 503.1 mL (range, 5.6–2242 mL), and the median OS was 12.9 months (95% confidence interval [CI]: 8.7, 16.1 months). There was a significant correlation between tDV and established prognostic factors, including hemoglobin level ($r = -0.521$, $P < .001$), prostate-specific antigen level ($r = 0.556$, $P < .001$), lactate dehydrogenase level ($r = 0.534$, $P < .001$), alkaline phosphatase level ($r = 0.572$, $P < .001$), circulating tumor cell count ($r = 0.613$, $P = .004$), and BSI ($r = 0.565$, $P = .001$). A higher tDV also showed a significant association with poorer OS (hazard ratio, 1.74; 95% CI: 1.02, 2.96; $P = .035$).

Conclusion: Metastatic bone disease from mCRPC can be evaluated and quantified with whole-body DW imaging. Whole-body DW imaging–generated tDV showed correlation with established prognostic biomarkers and is associated with OS in mCRPC.

© RSNA, 2016

Online supplemental material is available for this article.

Prostate cancer is the second most common cancer and the fifth leading cause of cancer death among men worldwide (1). Prostate cancer metastasizes primarily to the bone; skeletal dissemination occurs in up to 84% of patients (2), causing higher morbidity and mortality in this population (3–5). Despite notable advances in the management of metastatic castration-resistant prostate carcinoma (mCRPC) with new drugs, including abiraterone acetate and enzalutamide, which have been approved in the past 5 years (6,7), mCRPC remains ultimately a fatal condition. Current bone imaging is inadequate, relying largely on bone scintigraphy with technetium 99m, an isotope taken up primarily by osteoblasts that is unable to accurately depict and quantify the true extent of metastatic disease to bone. The development of quantitative imaging biomarkers that can accurately evaluate the burden of bone metastases may help individualize patient risk stratification and treatment selection and may ultimately be useful for evaluating the response to treatment.

The accuracy of magnetic resonance (MR) imaging in the detection of bone metastases is higher than that of bone scintigraphy and, possibly, choline positron emission tomography (PET)/computed tomography (CT) (8,9). Moreover, functional MR imaging complements anatomic sequences that assess some biologic characteristics of the tumor. Diffusion-weighted (DW) imaging is a functional MR imaging technique that provides quantitative measurement of the random displacement of water molecules (10). Previous studies have established the high sensitivity of DW imaging in the identification of bone metastases (11,12). DW imaging also allows easy delineation of areas of signal abnormality with semiautomated segmentation software; this provides the opportunity to more accurately determine the true extent of bone metastases. In addition, the apparent diffusion coefficient (ADC) shows correlation with cell density in different tumor types, including prostate cancer (13–17).

As part of a broader effort to clinically qualify whole-body MR imaging of bone metastases for mCRPC, our study was conducted to determine the correlation between volume of bone metastasis as assessed with DW imaging and established prognostic factors in mCRPC and the association of volume of bone metastases with overall survival (OS).

Materials and Methods

This retrospective study was approved by the institutional review board. Verbal informed consent was obtained for the acquisition of the MR images, and written informed consent was obtained for the acquisition of biologic samples from all patients.

Patient Population

Fifty-four male patients with mCRPC who were receiving treatment at a single institution underwent whole-body MR imaging, including DW imaging, between June 2010 and February 2013 before starting a new line of anticancer therapy. Patients were included in the study if *(a)* whole-body MR imaging was performed within 4 weeks of starting a new line of anticancer therapy, *(b)* bone metastases were identified on the basis of a review of images from combined imaging modalities (MR imaging, CT [in all cases], and bone scintigraphy [when available]), *(c)* whole-body MR imaging was performed with a 1.5-T unit (according to the technical parameters described below), and *(d)* at least 1 year of clinical follow-up data were available (or the patient died during the follow-up period). Patients were excluded if assessment with MR imaging was suboptimal owing to artifacts or incomplete studies. Of 54 cases reviewed, 43 were eligible for our study (all men; mean age, 69 years; age range, 41–80 years). The mean time between MR imaging and the start of treatment was 2.2 weeks. One case was not included

Advances in Knowledge

- Semiautomated whole-body diffusion-weighted (DW) imaging signal abnormality delineation is feasible, enabling the assessment of the total volume of bone metastasis in patients with metastatic castration-resistant prostate cancer (mCRPC).

- Assessment of total volume of bone metastasies with whole-body DW imaging informs on the overall survival of patients with mCRPC.

- In our data set, the volume of bone metastases assessed with whole-body DW imaging showed correlation with established prognostic biomarkers for patients with advanced mCRPC, including circulating tumor cell count.

Implication for Patient Care

- Assessment of the volume of bone metastases with whole-body DW imaging in patients with mCRPC may help individualize patient risk stratification and, therefore, treatment selection.

Radiology

because whole-body MR imaging was not performed within 4 weeks of starting a new line of treatment, six cases were excluded because there was no radiologic evidence of bone metastases, and four cases were excluded because of the presence of artifacts (eg, susceptibility artifacts) and/or incomplete studies (Fig 1).

Clinical Data Collection

Data were collected into an anonymized database. Patient characteristics included age, previous anticancer treatments, Eastern Cooperative Oncology Group performance status (18), and laboratory results (hemoglobin, prostate-specific antigen, lactate dehydrogenase, alkaline phosphate, and albumin levels) at the time of MR imaging. Circulating tumor cell (CTC) count (19) and bone scan index (BSI) were included only if obtained within 12 weeks of MR imaging (mean time from CTC count to MR imaging, 3.6 weeks; mean time from BSI to MR imaging, 3.0 weeks). Follow-up data collected from electronic patient records included survival status and OS (defined as time from MR imaging to death by any cause). For noncensored patients, follow-up data included the length of clinical follow-up.
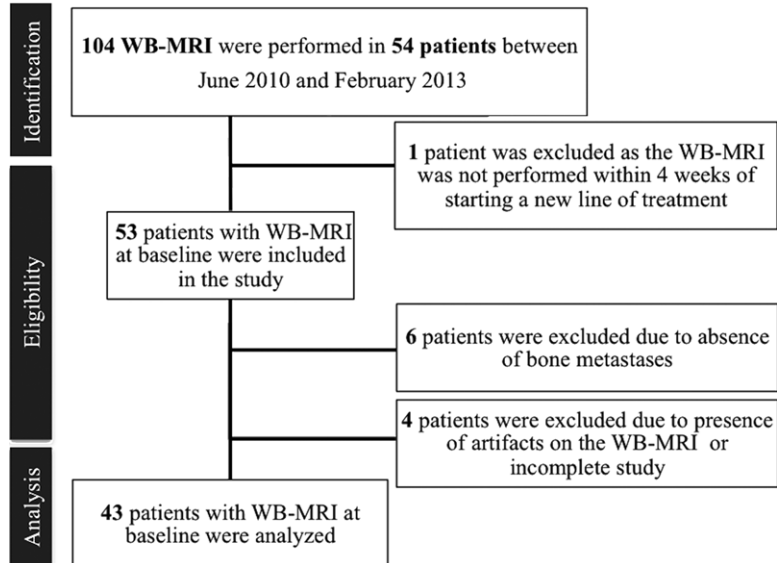
Whole-Body MR Imaging Parameters

MR imaging was performed with patients in the supine position by using a 1.5-T unit (Avanto; Siemens Healthcare, Erlangen, Germany) with surface and body coils. Axial images were acquired by using free-breathing single-shot twice-refocused echo-planar DW imaging from vertex to midthighs, sequentially across four imaging stations, with each consisting of 50 sections. In addition to whole-body DW imaging, anatomic imaging was also performed by using a breath-hold axial T1-weighted sequence. The imaging parameters used to perform whole-body MR imaging are summarized in Table 1.

Image Analysis

Images were processed and analyzed with open-access imaging assistant software (OsiriX v5.6; OsiriX Foundation,

Figure 1

Figure 1: Flowchart of study selection process. *WB* = whole body.

Table 1

Imaging Parameters for Whole-Body DW Imaging

Parameter	T1-weighted Imaging	DW Imaging
Type of pulse sequence	Spoiled gradient echo (FLASH)	Single-shot twice-refocused echo-planar imaging
Respiration	Breath hold	Free breathing
Type of acquisition	2D	2D
Field of view (mm)	380–420	380–420
Repetition time (msec)	380	14 000
Echo time (msec)	5	68
Inversion time (msec)	NA	180
Flip angle (degrees)	70	90
Fat suppression	NA	STIR
Receiver bandwidth (Hz/pixel)	331	1800
No. of signals acquired	1	4
Section thickness (mm)	5	5
b value (sec/mm^2)	NA	50 and 900
No. of stations	4 (from vertex to midthighs), 50 sections each	4 (from vertex to midthighs), 50 sections each

Note.—A 1.5-T unit (Avanto, Siemens Healthcare) was used for the imaging platform. FLASH = fast low-angle shot, NA = not applicable, STIR = short inversion time inversion recovery, 2D = two-dimensional.

Geneva, Switzerland). The T1-weighted and DW images (b value = 50 and 900 sec/mm^2 and ADC maps) were evaluated to assess the presence of metastatic bone disease. Regions of interest including all areas of signal intensity abnormality on DW images obtained with a b value of 900 sec/mm^2, which corresponded to

high signal intensity on DW images obtained with a b value of 900 sec/mm^2 and low signal intensity on T1-weighted images, in keeping with metastatic bone disease, observed between C4 and midthighs were delineated. The skull vault and base were excluded owing to frequent artifacts, poor visualization of

disease, and lower incidence of metastases in these locations (20). A semiautomatic segmentation tool from the OsiriX software was used for delineating bone disease. The delineation of total tumor diffusion volume (tDV) was performed by a radiologist (R.P.L.) with 2 years of experience in whole-body DW imaging; manual correction of the segmentation mask corresponding to the volume of interest was performed when necessary (Fig 2). Pixel size and number of pixels for all volumes of interest were recorded to calculate the tDV for each patient. The ADC of every pixel was recorded, and

histogram representations of the ADCs of tDV for each patient were generated by using software (Excel 2010; Microsoft, Redmond, Wash).

Parameters analyzed at whole-body DW imaging included the tDV (defined as the number of pixels multiplied by the pixel volume in each case, accounting for differences in the size of the field of view), mean, median, skewness, and kurtosis of the ADC histogram for each patient.

A randomly selected subset of 10 cases was analyzed again by the primary radiologist (R.P.L.) at least 6 months

after the first assessment and by a second radiologist (N.T., with 6 years of experience in whole-body DW imaging) who was blinded to the initial analysis with the purpose of assessing the intra- and interobserver reliability in tDV measurement.

CTC Count

CTCs were enumerated after isolation from blood samples by using a tumor cell kit (Cellsearch system; Janssen Diagnostics, Raritan, NJ), as described in a previous article (21). Results are expressed as the number of CTCs per 7.5 mL of blood.
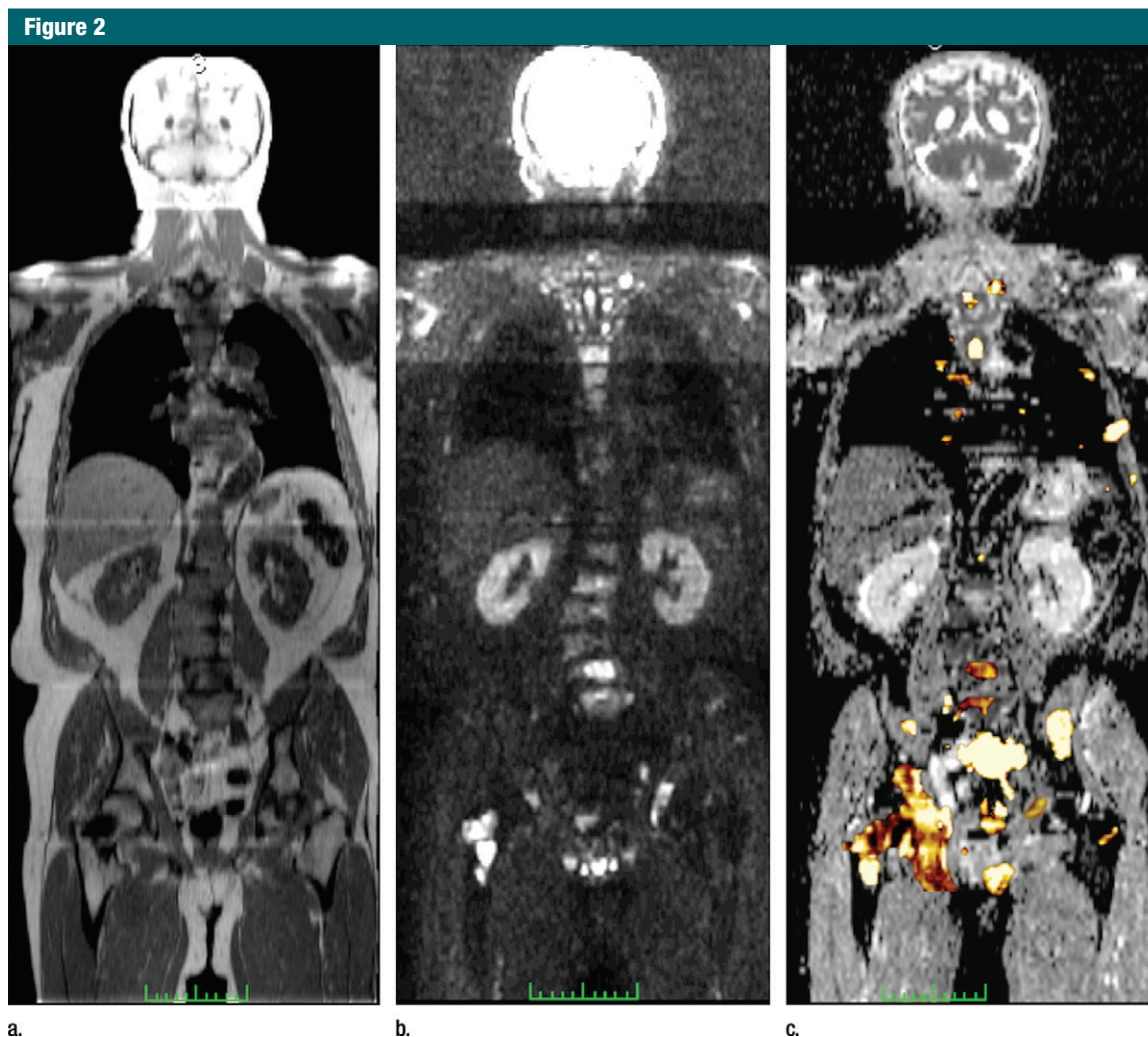
Figure 2

Figure 2: Images show metastatic bone disease segmentation steps in two-dimensional coronal views for illustrative purpose. Areas of signal abnormality corresponding to **(a)** high signal intensity on DW image ($b = 900$ mm/sec^2) and **(b)** low signal intensity on T1-weighted image, in keeping with bone metastases observed between C4 and the midthigh, were delineated and applied to the ADC map **(c)** to obtain ADCs in areas of interest. The overlaid colored mask is a three-dimensional representation of the tumor volume accounting for the apparent mismatch.

Table 2

Baseline Characteristics and Previous Treatments of the Overall Population Included in the Final Analysis

Parameter	Value*
Baseline clinical characteristics (*n* = 43)[†]	
Hemoglobin level (g/dL)	43 [11] (10–13)
Prostate-specific antigen level (ng/mL)	43 [222] (69–1486)
Alkaline phosphatase level (IU/L)	43 [140] (88–586)
Lactate dehydrogenase level (IU/L)	43 [183] (151–247)
Albumin level (g/dL)	43 [37] (32–39)
BSI	32 [7.9] (2–11.5)
CTC count (cells per 7.5 mL of blood)	21 [35] (7–148)
Prior treatments[‡]	
Docetaxel	29 (67.4)
Cabazitaxel	10 (23.3)
Abiraterone acetate	27 (62.8)
Enzalutamide	7 (16.3)
Radium-223	1 (2.3)
Bisphosphonates	6 (14)
Palliative radiation therapy to bone	22 (51.2)
Sites of metastatic disease[‡]	
Bone only	20 (46.5)
Bone and nodal	17 (39.5)
Bone and viscera	6 (14)
Metastatic bone disease characteristics	
Median tDV (mL)[§]	503.1 (5.6–2242)
Median ADC (x10^{-6} mm^2/sec)[‖]	813 (780, 906)
Median OS (mo)[‖]	12.9 (8.7, 16.1)

* Unless otherwise specified, data are numbers of patients.

[†] Numbers in brackets are medians. Numbers in parentheses are the IQR.

[‡] Numbers in parentheses are percentages.

[§] Numbers in parentheses are the range.

[‖] Numbers in parentheses are 95% CIs.

BSI Calculation

For those patients who underwent bone scintigraphy within 12 weeks of MR imaging and for whom Digital Imaging and Communication in Medicine images were available, the BSI was calculated by using an automated BSI scoring software system (Exini Diagnostics, Lund, Sweden) (22).

Statistical Analysis

The Pearson correlation coefficient (*r*) was determined to establish the correlation between variables. Kaplan-Meier analysis was used to study the OS of the population. Patients who were alive at the time of last follow-up were censored. Cox proportional hazards models were used to determine the association of the variables with OS. The comparison between the discriminative ability of MR imaging and bone scintigraphy in the prediction of OS was performed by assessing the status of each patient (dead vs alive) at several time points (9, 12, and 15 months) and determining the area under the receiver operating characteristic curve (concordance index, or C-index). Comparison between receiver operating characteristic curves was performed with the method established by DeLong et al (23). The 95% confidence interval (CI) of the median ADC of the entire population was calculated by means of bootstrapping. tDV, BSI, prostate-specific antigen level, CTC count, alkaline phosphate level, and lactate dehydrogenase level were log-transformed to account for the lack of normal distribution. The intra- and interobserver reliability of tDV measurements were assessed by using the Lin concordance correlation coefficient of absolute agreement and Bland-Altman analysis. Limits of agreement were defined as the mean difference ± 1.96 times the standard deviation of the differences. The coefficient of repeatability was calculated as 1.96 times the standard deviation of the differences between the two measurements. Software (SPSS, version 20; IBM, Armonk, NY) was used for statistical analyses.

Results

Forty-three patients were eligible and included in the analysis. Twenty of the 43 patients (46.5%) had metastatic disease limited to bone, 17 (39.5%) had bone and nodal disease, and six (14%) had visceral disease in addition to bone metastases.

Patients in our dataset had received a median of three (range, 0–7) lines of treatment for mCRPC at the time of MR imaging, including four patients (9.3%) who were treatment-naïve for mCRPC in whom MR imaging was performed within 4 weeks before their first systemic treatment for mCRPC. Twenty-eight of the 43 patients (65.1%) had undergone previous treatment with at least abiraterone acetate and/or enzalutamide and 29 (67.4%) were previously treated with taxane-based chemotherapy.

Thirty of the 43 patients (69.8%) died during the follow-up period, with 13 patients (30.2%) alive at the time of data analysis. The median OS of the overall population was 12.9 months (95% CI: 8.7, 16.1 months), with a median follow-up of 11.1 months (interquartile range [IQR]: 7.4–15.7 months). Patient and tumor characteristics, including treatment received before inclusion in our study, are summarized in Table 2.

The median tDV was 503.1 mL (range, 5.6–2242 mL), with a median global ADC for the regions of interest

Figure 3
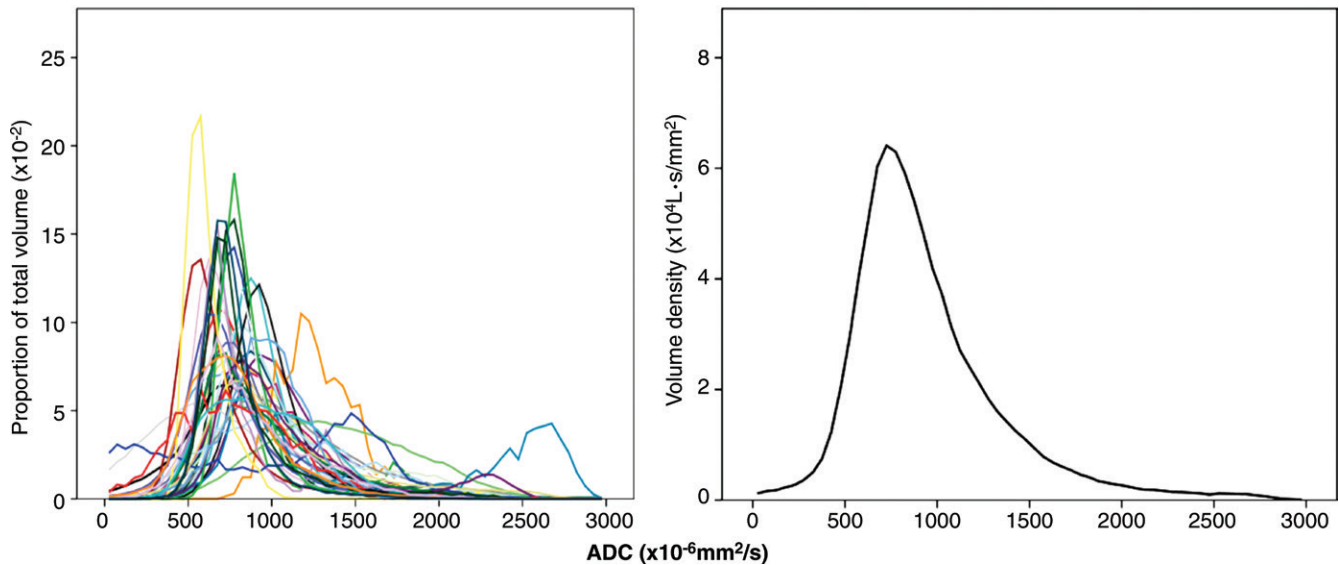
Figure 3: Left, histogram representation of ADCs for every patient included in analysis ($n = 43$). Right, volume density plot, where the y-axis represents the volume density per unit ADC. The area under the curve thus represents the total volume of disease in the patient population.

for each individual of 813×10^{-6} mm²/sec (95% CI: 780, 906 $\times 10^{-6}$ mm²/sec), median skewness of 1.5 (IQR: 0.9–1.9), and median kurtosis of 3.5 (IQR: 1.4–7). Histograms of the global ADCs for each patient and the whole population are shown in Figure 3. Two patients had bimodal histograms, with a high density of ADCs within 500–1500 $\times 10^{-6}$ mm²/sec and a smaller peak within 2000–3000 $\times 10^{-6}$ mm²/sec. Both cases corresponded to patients who received focal palliative radiation therapy to the pelvis during the 6 months before MR imaging (Fig 4).

Correlation of tDV with Prognostic Factors

We investigated the correlation between tDV and known established prognostic factors, with special interest in those associated with bone disease (eg, hemoglobin and alkaline phosphate levels). Overall, tDV showed a significant correlation with all of the studied established prognostic factors for mCRPC (hemoglobin level: $r = -0.521$, $P < .001$; prostate-specific antigen level: $r = 0.556$, $P < .001$; lactate dehydrogenase level: $r = 0.534$, $P < .001$; and alkaline phosphate level: $r = 0.572$, $P < .001$) (Table 3).

Next, we explored the correlation between tDV and CTC count. Baseline CTC counts were available for 21 of the 43 patients (48.8%). The median CTC count was 35 cells per 7.5 mL (IQR: 7–148 cells per 7.5 mL). CTC count showed significant correlation with tDV ($r = 0.613$, $P = .004$), which is consistent with published evidence that high CTC count informs on worse prognosis in mCRPC (24) (Fig 5).

Association of tDV with OS

We hypothesized that the burden of bone disease would associate with OS in patients with mCRPC; tDV, as a continuous variable, showed a statistically significant association with OS, with patients with a higher tDV having an increased risk of death (hazard ratio: 1.74; 95% CI: 1.02, 2.96; $P = .035$).

### Association of Other Parameters Derived from Whole-Body DW Imaging with OS

Histogram parameters that describe the distribution of the global ADCs of bone metastases, such as mean (hazard ratio: 1; 95% CI: 0.998, 1.001; $P = .876$), median (hazard ratio: 1; 95% CI: 0.998, 1.002; $P = .928$), skewness (hazard ratio: 0.92; 95% CI: 0.563, 1.504; $P = .740$), or kurtosis (hazard ratio:

0.97; 95% CI: 0.89, 1.06; $P = .532$) did not show a significant association with OS in our population.

Comparison of the Predictive Ability of Whole-Body DW Imaging and BSI

Among the 43 patients, 32 (74.4%) had BSI data available for analysis from bone scans obtained within the prespecified time ranges. Seven of the 43 patients (16.3%) underwent bone scintigraphy more than 12 weeks apart from MR imaging and were therefore excluded from this subanalysis. Two of the 43 patients (4.7%) did not have results from bone scintigraphy available, and two (4.7%) did not have Digital Imaging and Communications in Medicine images, which are necessary for BSI calculation, available. The median BSI was 7.9 (IQR, 2–11.5). The tDV measured with whole-body DW imaging, as a continuous variable, and the estimation relative to total skeletal mass by the BSI were highly correlated ($r = 0.565$, $P = .001$) (Fig 5). To further assess the prognostic performance of BSI and tDV, we evaluated mortality rates at 9, 12, and 15 months (when approximately one-third, one-half, and two-thirds of patients had died). Receiver operating characteristic

Radiology

Figure 4

a.

b.

c.
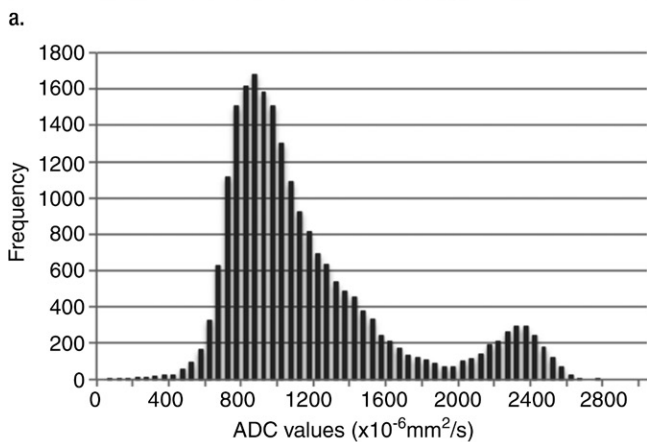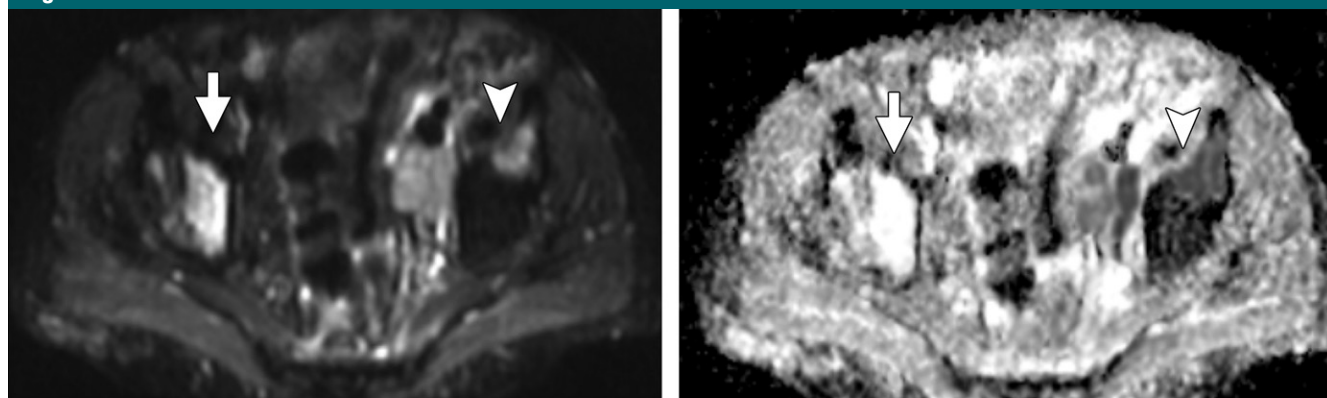
Figure 4: Images in 71-year-old man with mCRPC who underwent whole-body DW imaging in October 2012. He had received radiation therapy to right hemi-pelvis in June 2012. **(a)** Axial whole-body DW image ($b = 900$ mm/sec^2), **(b)** ADC map, and **(c)** histogram representation of ADCs show bimodal distribution with areas of high signal intensity on DW image and low ADC (arrowhead), in keeping with active and/or cellular disease, and areas of high signal intensity on DW image and high ADC (arrow) that represent treated and/or less-cellular disease.

Table 3

Correlation of tDV and Other Prognostic Factors

Prognostic Factor	Correlation Coefficient*	P Value
Hemoglobin level	−0.521	<.001
Prostate-specific antigen level	0.556	<.001
Lactate dehydrogenase level	0.534	<.001
Alkaline phosphatase level	0.572	<.001
Albumin level	−0.332	.030
CTC count	0.613	.004

Note.—The tDV, prostate-specific antigen level, lactate dehydrogenase level, alkaline phosphate level, and CTC count were log-transformed.

* Pearson correlation coefficient.

curve analysis was performed to determine the C-statistic (area under the receiver operating characteristic curve) with each of both imaging biomarkers at the specified time points. Although the area under the receiver operating characteristic curve for tDV was consistently superior to that for BSI for 9-month (0.745 vs 0.613, respectively; $P = .141$), 12-month (0.686 vs 0.627; $P = .533$), and 15-month (0.704 vs 0.607; $P = .345$) mortality rates (Fig E1 [online]), these differences were not statistically significant.

Intra- and Interobserver Reliability of tDV Measurement

The intraclass correlation coefficients were 0.986 (95% CI: 0.945, 0.996) and 0.949 (95% CI: 0.857, 0.981) for intra- and interobserver comparison, respectively. The Bland-Altman–calculated intraobserver coefficient of repeatability was 0.302 L, and the interobserver coefficient of repeatability was 0.500 L.

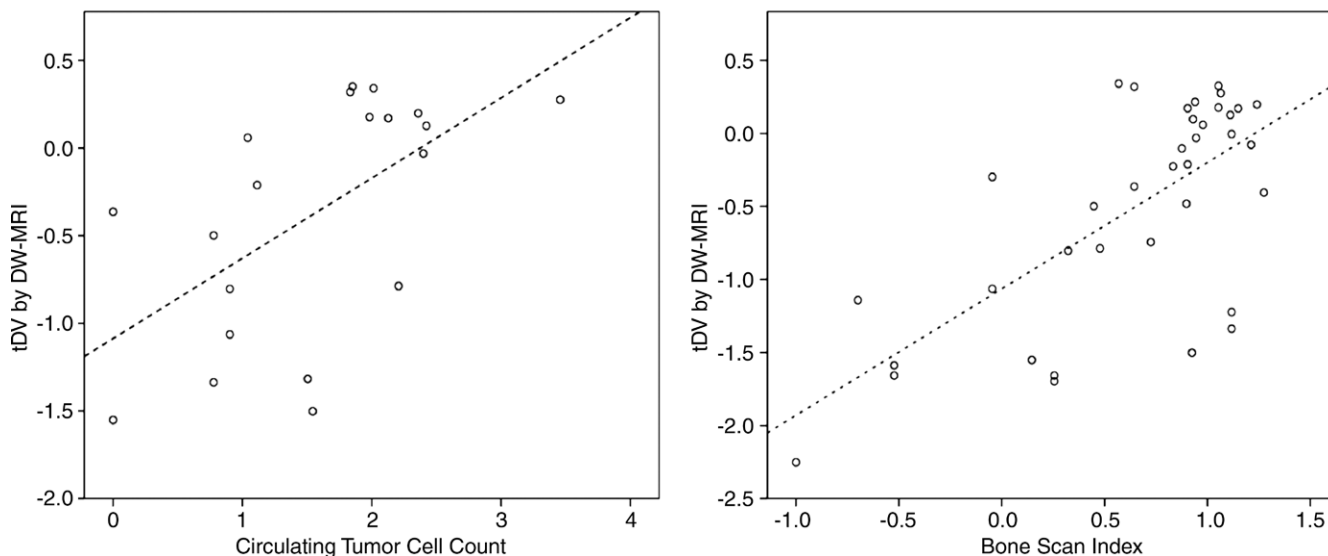All values in the intra- and interobserver Bland-Altman analysis are within the 95% limits of agreement.

Discussion

Bone involvement in patients with advanced prostate cancer is extremely common, resulting in higher morbidity and mortality in patients with mCRPC. When we consider the limitations of CT and bone scintigraphy in the accurate assessment of the extent of bone metastases, it is imperative to develop new imaging biomarkers and pursue their analytical and clinical quantification, with the aim of providing new tools for guiding radiologists and clinicians in therapeutic decisions.

Our study shows an association between whole-body DW imaging parameters, OS, and prognostic factors in mCRPC, which was previously

Figure 5

Figure 5: Scatterplots show relationship between tDV and CTC count and between tDV and BSI.

established in the literature. Notably, the volume of bone metastasis quantified with whole-body DW imaging correlates with prognostic biomarkers routinely implemented into standard physician's practice, such as hemoglobin level, prostate-specific antigen level, and the bone turnover marker alkaline phosphate level. Interestingly, we also detected a correlation with CTC count, an established prognostic biomarker in mCRPC, although these findings must be corroborated in larger populations.

Histogram representation of the ADCs of the burden of metastatic bone disease may also provide a useful representation of tissue cellularity. The median ADC for our population was 813×10^{-6} mm^2/sec; this value is lower than the median ADC reported in previous studies in other tumor types, including multiple myeloma (25), a disease with predominately lytic disease. In this mCRPC population, conversely, metastases were mainly sclerotic (26). Studies in which DW imaging is used as a biomarker in cancer medicine, therefore, must account for such differences in disease biology among tumor types. Furthermore, bimodal histograms reflect the coexistence of two different patterns

of disease with different cellular density distributions (27).

Parameters that help describe the distribution of the global ADCs of bone metastases, such as mean, median, skewness, or kurtosis, were not associated with OS in our population.

In the past few years it has been shown that indirect measurements of the burden of bone metastases, measured either as proportion of skeletal mass with BSI or the number of lesions visible at CT and PET/CT, provide prognostic information in prostate cancer (28,29). These examinations, however, only largely reflect bone turnover as a response to either benign or malignant processes. MR imaging has been previously shown to have higher sensitivity and specificity than bone scintigraphy and CT in the detection of bone metastases (12). In our data set, the receiver operating characteristic curves with bone scintigraphy were consistently inferior to those with whole-body DW imaging in the prediction of mortality, which suggests that the performance of DW imaging is superior. However, considering the limited population included in our study, formal comparisons in larger cohorts will be necessary to confirm this finding because the

differences did not reach statistical significance.

We acknowledge the potential limitations of our study. First, the retrospective observational nature of our work, the variability in the number and type of treatments administered in the time between MR imaging and the start of therapy, and the presence of nodal and visceral disease in some of our patients are limitations. Second, because of the limited sample size of our pilot study, it is important to note that we did not control for clinical factors in the evaluation of the association between tDV and OS. A larger population would be needed for future validation of these data, allowing for multivariate analysis—ideally in the setting of prospective studies. Third, there is a risk of underestimating the disease because the presented data included skeletal segmentation from the cervical spine to midthighs only. However, taking into account that the vast majority of bone metastases occur within the spine and pelvis (20), it is unlikely that this had a major effect on the assessment of the total burden of metastatic bone disease. Finally, it should be noted that delineation of the volume of interest is dependent on the quality of the acquired DW imaging data, the

semiautomatic segmentation tool, and radiologist expertise. Despite these limitations, to our knowledge, our study represents the largest series assessing mCRPC bone metastasis with DW imaging and the data presented herein support further evaluation of whole-body DW imaging in this disease.

One practical conclusion of our study is the demonstration of the feasibility of assessing metastatic bone disease from prostate cancer with whole-body DW imaging; indeed, in 49 of 53 cases reviewed (92%) the outcome of DW imaging was fully suitable for assessment. We are currently able to perform whole-body DW imaging in reasonably short data acquisition times (24 minutes), thus analyzing whole-tumor burden and its spatial heterogeneity. Other advantages of whole-body MR imaging including DW imaging compared with the current standard of CT and bone scintigraphy are the avoidance of the need for radiation or radioactive materials, evaluation of both soft-tissue and bone metastases, and accurate depiction of complications such as cord compression or bone fractures. Whole-body MR imaging including DW imaging can be implemented in everyday clinical practice, as the technique is robust and the protocols can be implemented in most of the commonly used imaging units.

In conclusion, we have shown a strong correlation between tDV assessed with whole-body DW imaging and proved prognostic factors in mCRPC, including CTC counts, and present promising data that support an association between tDV and OS. Our results, taken together with those from previous reports that describe changes in DW imaging after exposure to anticancer treatments (30), raise the need for further evaluation of DW imaging as a prognostic and response biomarker in prospective cohorts of patients with mCRPC to acquire clinical qualification and, eventually, implementation in routine clinical practice.

References

1. Ferlay J, Soerjomataram I, Dikshit R, et al. Cancer incidence and mortality worldwide: sources, methods and major patterns in GLOBOCAN 2012. Int J Cancer 2015;136(5):E359–E386.

2. Gandaglia G, Abdollah F, Schiffmann J, et al. Distribution of metastatic sites in patients with prostate cancer: a population-based analysis. Prostate 2014;74(2):210–216.

3. Carlin BI, Andriole GL. The natural history, skeletal complications, and management of bone metastases in patients with prostate carcinoma. Cancer 2000;88(12 Suppl):2989–2994.

4. Saad F, Lipton A, Cook R, Chen YM, Smith M, Coleman R. Pathologic fractures correlate with reduced survival in patients with malignant bone disease. Cancer 2007;110(8):1860–1867.

5. Sathiakumar N, Delzell E, Morrisey MA, et al. Mortality following bone metastasis and skeletal-related events among men with prostate cancer: a population-based analysis of US Medicare beneficiaries, 1999–2006. Prostate Cancer Prostatic Dis 2011;14(2):177–183.

6. de Bono JS, Logothetis CJ, Molina A, et al. Abiraterone and increased survival in metastatic prostate cancer. N Engl J Med 2011; 364(21):1995–2005.

7. Scher HI, Fizazi K, Saad F, et al. Increased survival with enzalutamide in prostate cancer after chemotherapy. N Engl J Med 2012;367(13):1187–1197.

8. Shen G, Deng H, Hu S, Jia Z. Comparison of choline–PET/CT, MRI, SPECT, and bone scintigraphy in the diagnosis of bone metastases in patients with prostate cancer: a meta-analysis. Skeletal Radiol 2014; 43(11):1503–1513.

9. Jambor I, Kuisma A, Ramadan S, et al. Prospective evaluation of planar bone scintigraphy, SPECT, SPECT/CT, (18)F-NaF PET/CT and whole body 1.5T MRI, including DWI, for the detection of bone metastases in high risk breast and prostate cancer patients: SKELETA clinical trial. Acta Oncol 2016;55(1):59–67.

10. Koh DM, Collins DJ. Diffusion-weighted MRI in the body: applications and challenges in oncology. AJR Am J Roentgenol 2007; 188(6):1622–1635.

11. Luboldt W, Küfer R, Blumstein N, et al. Prostate carcinoma: diffusion-weighted imaging as potential alternative to conventional MR and 11C-choline PET/CT for detection of bone metastases. Radiology 2008;249(3): 1017–1025.

12. Lecouvet FE, El Mouedden J, Collette L, et al. Can whole-body magnetic resonance imaging with diffusion-weighted imaging replace Tc 99m bone scanning and computed tomography for single-step detection of metastases in patients with high-risk prostate cancer? Eur Urol 2012;62(1):68–75.

13. Guo AC, Cummings TJ, Dash RC, Provenzale JM. Lymphomas and high-grade astrocytomas: comparison of water diffusibility and histologic characteristics. Radiology 2002;224(1):177–183.

14. Hayashida Y, Hirai T, Morishita S, et al. Diffusion-weighted imaging of metastatic brain tumors: comparison with histologic type and tumor cellularity. AJNR Am J Neuroradiol 2006;27(7):1419–1425.

15. Zelhof B, Pickles M, Liney G, et al. Correlation of diffusion-weighted magnetic resonance data with cellularity in prostate cancer. BJU Int 2009;103(7):883–888.

16. Liu Y, Ye Z, Sun H, Bai R. Clinical application of diffusion-weighted magnetic resonance imaging in uterine cervical cancer. Int J Gynecol Cancer 2015;25(6):1073–1078.

17. Matsubayashi RN, Fujii T, Yasumori K, Muranaka T, Momosaki S. Apparent diffusion coefficient in invasive ductal breast carcinoma: correlation with detailed histologic features and the enhancement ratio on dynamic contrast-enhanced MR images. J Oncol doi: 10.1155/2010/821048. Published online September 2, 2010. Accessed April 15, 2015.

18. Oken MM, Creech RH, Tormey DC, et al. Toxicity and response criteria of the Eastern Cooperative Oncology Group. Am J Clin Oncol 1982;5(6):649–655.

19. Olmos D, Arkenau HT, Ang JE, et al. Circulating tumour cell (CTC) counts as intermediate end points in castration-resistant prostate cancer (CRPC): a single-centre experience. Ann Oncol 2009;20(1): 27–33.

20. Kakhki VR, Anvari K, Sadeghi R, Mahmoudian AS, Torabian-Kakhki M. Pattern and distribution of bone metastases in common malignant tumors. Nucl Med Rev Cent East Eur 2013;16(2):66–69.

21. Kraan J, Sleijfer S, Strijbos MH, et al. External quality assurance of circulating tumor cell enumeration using the CellSearch(®) system: a feasibility study. Cytometry B Clin Cytom 2011;80(2):112–118.

22. Ulmert D, Kaboteh R, Fox JJ, et al. A novel automated platform for quantifying the extent of skeletal tumour involvement in prostate cancer patients using the bone scan index. Eur Urol 2012;62(1):78–84.

23. DeLong ER, DeLong DM, Clarke-Pearson DL. Comparing the areas under two or more correlated receiver operating characteristic curves: a nonparametric approach. Biometrics 1988;44(3):837–845.

24. de Bono JS, Scher HI, Montgomery RB, et al. Circulating tumor cells predict survival benefit from treatment in metastatic castration-resistant prostate cancer. Clin Cancer Res 2008;14(19):6302–6309.

25. Messiou C, Collins DJ, Morgan VA, Desouza NM. Optimising diffusion-weighted MRI for imaging metastatic and myeloma bone disease and assessing reproducibility. Eur Radiol 2011;21(8):1713–1718.

26. Messiou C, Collins DJ, Morgan VA, Bianchini D, de Bono JS, de Souza NM. Use of apparent diffusion coefficient as a response biomarker in bone: effect of developing sclerosis on quantified values. Skeletal Radiol 2014;43(2):205–208.

27. Padhani AR, van Ree K, Collins DJ, D'Sa S, Makris A. Assessing the relation between bone marrow signal intensity and apparent diffusion coefficient in diffusion-weighted MRI. AJR Am J Roentgenol 2013;200(1): 163–170.

28. Kaboteh R, Damber JE, Gjertsson P, et al. Bone scan index: a prognostic imaging biomarker for high-risk prostate cancer patients receiving primary hormonal therapy. EJNMMI Res 2013;3(1):9.

29. Vargas HA, Wassberg C, Fox JJ, et al. Bone metastases in castration-resistant prostate cancer: associations between morphologic CT patterns, glycolytic activity, and androgen receptor expression on PET and overall survival. Radiology 2014;271(1):220–229.

30. Blackledge MD, Collins DJ, Tunariu N, et al. Assessment of treatment response by total tumor volume and global apparent diffusion coefficient using diffusion-weighted MRI in patients with metastatic bone disease: a feasibility study. PLoS One 2014;9(4):e91779.